Düzce University Journal of Science & Technology

Research Article

The Effect of the Wall Thickness of the Material Loaded Cavity on the RCS Reduction

Oğuzhan DEMİRYÜREK [a,*], Filiz BİRBİR ÜNAL [a]

[a] *Department of Electrical Electronic Engineering, Faculty of Engineering, Düzce University, Düzce, TURKIYE*
** Corresponding author's e-mail address: oguzhandemiryurek@duzce.edu.tr*
DOI: 10.29130/dubited.1527024

ABSTRACT

In this paper, the effect of a parallel plate waveguide's wall thickness on radar cross-section reduction (RCS) is rigorously analyzed for H-polarization by using the Wiener-Hopf Technique, when the waveguide region is loaded with dielectric material and terminated with a perfect electric conductor (PEC) plate. Transfer matrices are incorporated into the analysis to account for the effect of different material layers through continuity relations. The Fourier transforms of the diffracted field and the boundary conditions yield a modified scalar Wiener-Hopf equation of the second kind (MWHE-2). The classical procedure to solve the MWHE-2 is applied and the approximate expression of the diffracted far field is obtained. Numerical results are given by comparing with the results available in the literature for the case of the wall thickness of the cavity not being considered.

Keywords: *RCS reduction, Wiener-Hopf Technique, Wall thickness of waveguide cavities*

Dielektrik Malzeme Yüklü Paralel Plaka Dalga Kılavuzu Duvar Kalınlığının RCS Azaltılmasına Etkisi

ÖZ

Bu çalışmada, paralel plaka dalga kılavuzunun duvar kalınlığının radar kesit alanının azalmasına (RCS) etkisi, dalga kılavuzu bölgesi dielektrik malzeme ile yüklendiğinde ve mükemmel iletken (PEC) bir levha ile sonlandırıldığında H-polarizasyonu için Wiener-Hopf Tekniği kullanılarak titizlikle analiz edilmiştir. Süreklilik bağıntıları kullanılırken, farklı malzeme katmanlarının etkisini hesaba katmak için transfer matrisleri analize dahil edilir. Kırınan alanın Fourier dönüşümünün ve sınır koşullarının kullanılması, ikinci türden değiştirilmiş bir skaler Wiener-Hopf denklemini (MWHE-2) verir. MWHE-2'yi çözmek için klasik prosedür uygulanır ve kırınıma uğrayan uzak alanın yaklaşık ifadesi elde edilir. Sayısal sonuçlar, literatürde mevcut olan paralel plaka dalga kılavuzunun duvar kalınlığının dikkate alınmadığı durumdaki sonuçlarla karşılaştırılarak verilmiştir.

Anahtar Kelimeler: *Radar kesit alanı azaltma, Wiener-Hopf Tekniği, Dalga kılavuzunun duvar kalınlığı*

Received: 02/08/2024, Revised: 26/08/2024, Accepted: 28/08/2024

I. INTRODUCTION

Reducing and predicting the radar cross-section (RCS) of objects or targets is a critical and important subject in electromagnetic wave scattering studies. Previously, scattering and diffraction properties of some simple geometric elements like edges, cylinders, spheres, plates, and shells have been analyzed to understand how to predict or reduce the RCS of complex objects such as vehicles or aircraft [1-9]. An important geometry to investigate is the open-ended parallel plate waveguide cavity, which forms a model for duct systems like jet engine intakes and many microwave elements such as filters, antennas, and transmission lines. There are a variety of papers studying two-dimensional or three-dimensional cavity problems using numerical or high-frequency ray techniques [10-14], however, the results may not apply to arbitrary cavity sizes.

The Wiener-Hopf technique has been used for a wide range of problems including finite or semi-infinite planar and cylindrical structures since it is a rigorous and efficient way of studying wave scattering and diffraction problems with canonical geometries [6, 15, 16]. The Wiener-Hopf technique can also be used with the mode matching method, which gives rise to the modified Wiener-Hopf equation that helps us analyze the effect of the thickness of the target and stack of dielectric layers. In previous studies, Kobayashi et al. used the Wiener-Hopf technique to conduct a rigorous RCS analysis of various two-dimensional cavities created by finite parallel-plate waveguides [16-20] and semi-infinite parallel-plate waveguides [16, 21-27], however, they didn't take into account the wall thickness of the parallel plates. Furthermore, the approach in [16-22] and [25, 26] results in a more sophisticated and extensive analysis each time they add a new dielectric material layer to the waveguide region.

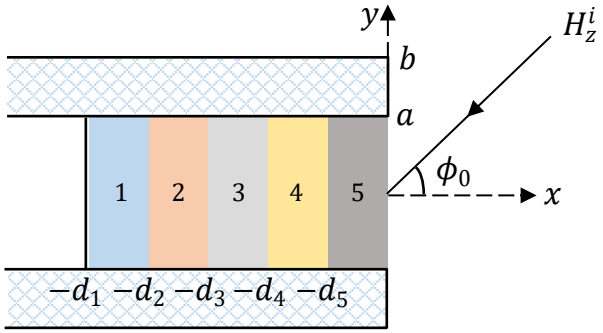

Figure 1. *Geometry of the investigated problem*

The paper is organized as follows. In Section II, the authors of this study examine the scattering that results from a thick parallel plate waveguide cavity, as shown in Figure 1, loaded with different numbers of layers of dielectric material in the case of H-polarization. As seen in Figure 1, the numbers 1, 2, 3, 4, 5 denote the number of layers of dielectric material. Constitutive parameter of the layer jth is ε_j, μ_j where j=1,2,…,5. By applying the Fourier transform technique to the scattered field components and the related boundary conditions, the problem reduces to a modified matrix Wiener-Hopf equation (WHE), but there is no general method to factorize an arbitrary matrix that appears in the WHE. Instead, incorporating a series of normal modes in the waveguide region for each dielectric layer, we obtain transfer matrices along with scalar modified Wiener-Hopf equation of the second kind. The solution contains infinitely many unknown constants that satisfy an infinite system of linear algebraic equations. A numerical solution of this system is presented in Section III, which compares the results of [25] for the same dielectric parameters and aperture sizes while taking into account the wall thickness of the waveguide. The paper concludes with a discussion of the effect of the wall thickness and the material properties of the dielectric layers in the cavity region.

In this study, time dependence is assumed as $e^{-i\omega t}$ where ω is the angular frequency, and is suppressed throughout the paper.

II. ANALYSIS

We consider the diffraction by a cavity formed by two thick semi-infinite PEC plates as shown in Figure 1 for an H_z-polarized plane wave. As seen in Figure 2 (a) and (b), one can proceed to decompose the incident wave into odd and even excitations to determine the scattered field. It is possible to show that the configurations in Figures 2 (a) and (b) are identical to those in Figures 2 (c) and (d), respectively, by using the image bisection principle. The odd and even excitations will be discussed separately in the sections that follow.

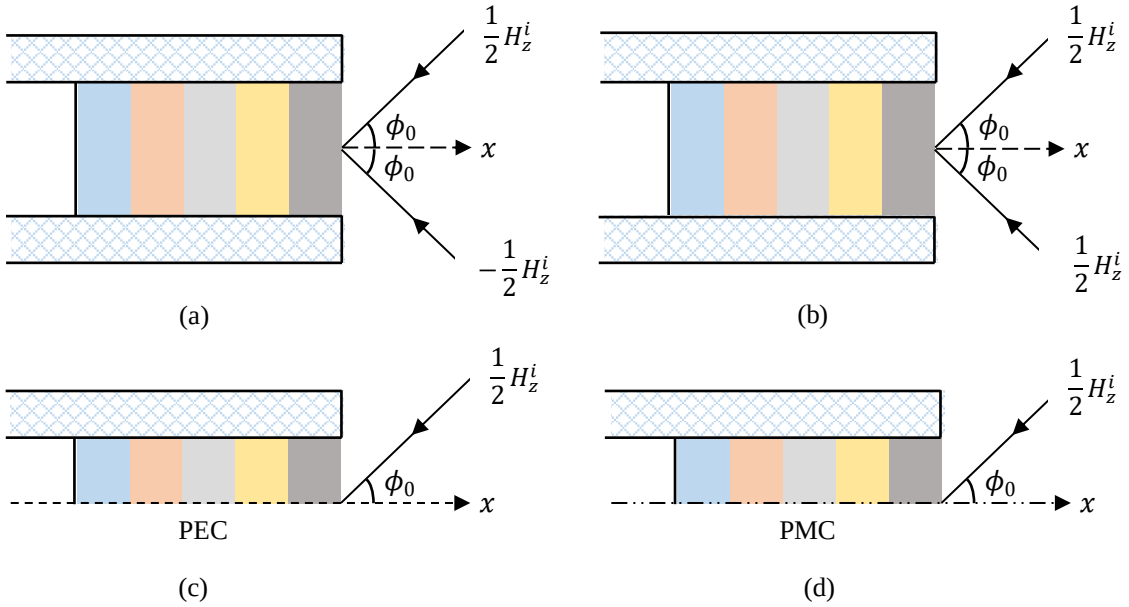

Figure 2. *Equivalent problems* ***(a)*** *Asymmetric (odd) excitation.* ***(b)*** *Symmetric (even) excitation.* ***(c)*** *Equivalence to* ***(a).*** ***(d)*** *Equivalence to* ***(b).***

A. ODD EXCITATION

First, we will look at the configuration shown in Figure 2(a), which corresponds to the odd excitation case. Since the field is not symmetrical about the plane $y = 0$ in this particular case, the total electric field for $x \in (-\infty, \infty)$ (electric wall) must vanish.

For analysis, the total field can be expressed as follows:

$$u^o(x,y) = \begin{cases} u^i + u^r + u_1^o, & y > b, x \in (-\infty, \infty) \\ u_{2,j}^o, & 0 < y < a, -d_j < x < -d_{j+1}, j = 1,2,\dots,5 \\ u_3^o, & a < y < b, x > 0 \end{cases} \quad (1)$$

Here, u^i is the incident field given by

$$H_z^i = u^i(x,y) = e^{-ik(x\cos\phi_0 + y\sin\phi_0)}, \quad (2a)$$

and u^r is the field reflected from the plane $y = b$, namely

$$u^r(x,y) = -e^{-ik(x\cos\phi_0 - (y-2b)\sin\phi_0)} \quad (2b)$$

with $k = \omega\sqrt{\varepsilon_0\mu_0}$ is the free-space wave number and ϕ_0 is the angle of the incident field. The total field satisfies the two-dimensional Helmholtz equation

$$\left[\frac{\partial^2}{\partial x^2}+\frac{\partial^2}{\partial y^2}+k^2\right]u^o(x,y)=0, \tag{3}$$

and is determined to satisfy the following boundary conditions and continuity relations:

$$\frac{\partial}{\partial y}u_1^o(x,b)=0, \qquad x<0 \tag{4a}$$

$$\frac{\partial}{\partial y}u_{2,j}^o(x,a)=0, \qquad x<0 \tag{4b}$$

$$u_{2,j}^o(x,0)=0, \qquad x<0 \tag{4c}$$

$$u_3^o(x,0)=0, \qquad x>0 \tag{4d}$$

$$u_1^o(x,b)-u_3^o(x,b)=-2e^{-ik(x\cos\phi_0+b\sin\phi_0)}, \qquad x>0 \tag{4e}$$

$$u_{2,1}^o(-d_1,y)=0, \qquad 0<y<a \tag{4f}$$

$$u_{2,j}^o\big(-d_{j+1},y\big)=u_{2,j+1}^o\big(-d_{j+1},y\big), \qquad 0<y<a \tag{4g}$$

$$\frac{1}{\varepsilon_j}\frac{\partial}{\partial x}u_{2,j}^o\big(-d_{j+1},y\big)=\frac{1}{\varepsilon_{j+1}}\frac{\partial}{\partial x}u_{2,j+1}^o\big(-d_{j+1},y\big), \qquad 0<y<a \tag{4h}$$

$$u_{2,5}^o(0,y)=u_3^o(0,y), \qquad 0<y<a \tag{4i}$$

$$\frac{\partial}{\partial x}u_3^o(0,y)=\begin{cases}\dfrac{1}{\varepsilon_5}\dfrac{\partial}{\partial x}u_{2,5}^o(0,y), & 0<y<a\\ 0, & a<y<b\end{cases} \tag{4j}$$

Since $u_1^o(x,y)$ satisfies Helmholtz equation in the region $y>b, x\in(-\infty,\infty)$, its Fourier transform with respect to x satisfies

$$\left[\frac{d^2}{dy^2}+(k^2-\alpha^2)\right]F^o(\alpha,y)=0 \tag{5a}$$

with

$$F^o(\alpha,y)=F_+^o(\alpha,y)+F_-^o(\alpha,y) \tag{5b}$$

where

$$F_+^o(\alpha,y)=\pm\int_0^{\pm\infty}u_1^o(x,y)e^{i\alpha x}dx\,. \tag{5c}$$

By considering the asymptotic behaviors of $u_1^o(x,y)$ for $x\to\pm\infty$

$$u_1^o(x,y)=\begin{cases}\mathcal{O}\big(e^{-ikx}\big), & x\to-\infty\\ \mathcal{O}\big(e^{-ikx\cos\phi_0}\big), & x\to\infty\end{cases}, \tag{6}$$

we can show that $F_+^o(\alpha,y)$ and $F_-^o(\alpha,y)$ are regular functions of α in the half-planes $\Im m(\alpha)>\Im m(k\cos\phi_0)$ and $\Im m(\alpha)<\Im m(k)$, respectively. The general solution of (5a) that satisfies the radiation condition for $y\to\infty$, gives

$$F_+^o(\alpha, y) + F_-^o(\alpha, y) = A^o(\alpha) e^{iK(\alpha)(y-b)}. \tag{7}$$

Here, $K(\alpha) = \sqrt{k^2 - \alpha^2}$ is the square root function defined in the complex α-plane cut along $\alpha = k$ to $\alpha = k + i\infty$ and $\alpha = -k$ to $\alpha = -k - i\infty$, as can be seen in Figure 3, such that $K(0) = k$. From (4a), we get $\dot{F}_-^o(\alpha, b) = 0$ in the Fourier transform domain, and the derivative of (7) with respect to y at $y = b$, one obtains

$$\dot{F}_+^o(\alpha, b) = iK(\alpha) A^o(\alpha) \tag{8}$$

$\dot{(\ )}$ denotes the derivative with respect to y.

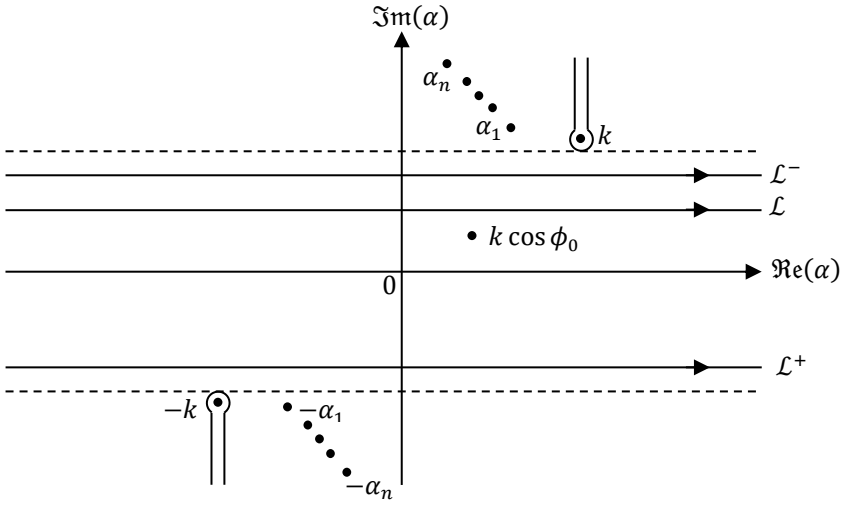

***Figure 3**. Brunch-cuts and integration lines in the complex plane*

In the region $x > 0,\ 0 < y < b$, $u_3^o(x, y)$ satisfies the Helmholtz equation and its half-range Fourier transform gives

$$\left[\frac{d^2}{dy^2} + [K(\alpha)]^2\right] G_+^o(\alpha, y) = f^o(y) + \alpha g^o(y) \tag{9a}$$

with

$$f^o(y) = \frac{\partial}{\partial x} u_3^o(0, y), \qquad g^o(y) = -i u_3^o(0, y). \tag{9b}$$

$G_+^o(\alpha, y)$ is defined by

$$G_+^o(\alpha, y) = \int_0^\infty u_3^o(x, y) e^{i\alpha x} dx\,. \tag{9c}$$

The general solution of (9a) satisfying the boundary condition at $y = 0$ gives

$$\begin{aligned} G_+^o(\alpha, y) = \ & \frac{\sin Ky}{KM^o(\alpha)} \left\{ \dot{F}_+^o(\alpha, b) - \int_0^b [f^o(t) + \alpha g^o(t)] \cos K(b - t)\, dt \right\} \\ & + \frac{1}{K(\alpha)} \int_0^y [f^o(t) + \alpha g^o(t)] \sin K(y - t)\, dt \end{aligned} \tag{10a}$$

with

$$M^o(\alpha) = \cos Kb. \tag{10b}$$

Although the left-hand side of (10a) is regular in the upper half-plane $\Im m\{\alpha\} > \Im m\{-k\}$, the regularity of the right-hand side is violated by the presence of simple poles occurring at $\alpha = \alpha_m^o$ which are zeros of $M^o(\alpha)$, satisfying

$$M^o(\alpha_m^o) = 0, \qquad K_m^o = K(\alpha_m^o) = \frac{(2m+1)\pi}{2b}, \qquad m = 0,1,2,\ldots \tag{11}$$

These poles can be eliminated by imposing that their residues are zero. This gives

$$\dot{F}_+^o(\alpha_m^o, b) = \frac{b}{2}\sin K_m^o b\,(f_m^o + \alpha_m^o g_m^o) \tag{12a}$$

where

$$\begin{bmatrix} f_m^o \\ g_m^o \end{bmatrix} = \frac{2}{b}\int_0^b \begin{bmatrix} f^o(t) \\ g^o(t) \end{bmatrix} \sin K_m^o t\, dt \tag{12b}$$

Taking into account (7), (8), (10a), (12b) and evaluating the resultant integral, one obtains the MWHE-2 valid in the strip $\Im m(k\cos\phi_0) < \Im m(\alpha) < \Im m(k)$,

$$\frac{\dot{F}_+^o(\alpha, b)}{iK(\alpha)N^o(\alpha)} - F_-^o(\alpha, b) = -\frac{2ie^{-ikb\sin\phi_0}}{(\alpha - k\cos\phi_0)} + \sum_{m=0}^{\infty}(f_m^o + \alpha g_m^o)\frac{\sin K_m^o b}{K^2 - (K_m^o)^2} \tag{13a}$$

with

$$N^o(\alpha) = M^o(\alpha)\, e^{iK(\alpha)b}. \tag{13b}$$

$N^o(\alpha)$ is the kernel function of (13a) and factorized as [27]

$$N^o(\alpha) = N_+^o(\alpha)N_-^o(\alpha) \tag{14a}$$

$$N_+^o(\alpha) = N_-^o(-\alpha) \tag{14b}$$

where

$$\begin{aligned} N_+^o(\alpha) = {} & \sqrt{\cos kb}\ \exp\left\{\frac{ib\alpha}{\pi}\left(1 - C + \ln\left(\frac{\pi}{2kb}\right) + i\frac{\pi}{2}\right)\right\} \\ & \times \exp\left\{\frac{ibK}{\pi}\ln\left(\frac{\alpha + K}{k}\right)\right\}\prod_{m=1}^{\infty}\left(1 + \frac{\alpha}{\alpha_m}\right)\exp\left\{\frac{i\alpha b}{m\pi}\right\} \end{aligned} \tag{14c}$$

with $C = 0.57721566\ldots$ being Euler's constant. WHE in (13a) is solved by following the classical procedure and one gets

$$\frac{\dot{F}_+^o(\alpha, b)}{iN_+^o(\alpha)\sqrt{k+\alpha}} = \tilde{F}_+^o(\alpha, b), \tag{15a}$$

where

$$\tilde{F}_{+}^{o}(\alpha,b)=-2ie^{-ikb\sin\phi_0}\frac{\sqrt{k(1-\cos\phi_0)}\,N_{-}^{o}(k\cos\phi_0)}{(\alpha-k\cos\phi_0)}+\sum_{m=0}^{\infty}\frac{(f_m^o-\alpha_m^o g_m^o)}{2\alpha_m^o}\frac{N_{+}^{o}(\alpha_m^o)\sqrt{k+\alpha_m^o}\,\sin K_m^o b}{(\alpha+\alpha_m^o)}. \tag{15b}$$

Consider now the waveguide region $x<0, 0<y<a$. Since the waveguide region has more than one material layer, $u_{2,j}^{o}(x,y)$ should be expressed separately for each layer. The field in each layer can be given as

$$u_{2,j}^{o}(x,y)=\sum_{n=0}^{\infty}\left[b_{n,j}^{o}e^{i\beta_{n,j}^{o}x}+c_{n,j}^{o}e^{-i\beta_{n,j}^{o}x}\right]\sin\gamma_n^o y\,,\qquad j=1,2,\dots,5 \tag{16a}$$

$$\gamma_n^o=\frac{(2n+1)\pi}{2a},\qquad n=0,1,2,\dots \tag{16b}$$

$$\beta_{n,j}^{o}=\sqrt{k_j^2-(\gamma_n^o)^2} \tag{16c}$$

where $k_j=k\sqrt{\varepsilon_j\mu_j}$, j denotes the jth layer.

The field $u_{2,1}^{o}(x,y)$ valid in the region $x\in(-d_1,-d_2)$ and satisfying the boundary condition at $x=-d_1$ can be written as follows:

$$u_{2,1}^{o}(x,y)=\sum_{n=0}^{\infty}b_{n,1}^{o}\cos\beta_{n,1}^{o}(x+d_1)\sin\gamma_n^o y. \tag{17}$$

When we consider the continuity relations (4g) and (4h) between the dielectric layers and substitute the field expressions $u_{2,j}^{o}(x,y)$ into them, we get

$$\mathbf{T}_1^o b_{n,1}^o=\mathbf{T}_{2,2}^o\mathbf{x}_{n,2}^o \tag{18a}$$

$$\mathbf{T}_{j-1,j}^o\mathbf{x}_{n,j-1}^o=\mathbf{T}_{j,j}^o\mathbf{x}_{n,j}^o,\qquad j=3,4,5, \tag{18b}$$

where we define

$$\mathbf{x}_{n,j}^o=\begin{bmatrix}b_{n,j}^o\\c_{n,j}^o\end{bmatrix} \tag{18c}$$

$$\mathbf{T}_1^o=\begin{bmatrix}\cos\beta_{n,1}^o(d_1-d_2)\\-\frac{\beta_{n,1}^o}{\varepsilon_1}\sin\beta_{n,1}^o(d_1-d_2)\end{bmatrix} \tag{18d}$$

$$\mathbf{T}_{j-1,j}^o=\begin{bmatrix}e^{-i\beta_{n,j-1}^o d_j} & e^{i\beta_{n,j-1}^o d_j}\\\frac{i\beta_{n,j-1}^o}{\varepsilon_{j-1}}e^{-i\beta_{n,j-1}^o d_j} & -\frac{i\beta_{n,j-1}^o}{\varepsilon_{j-1}}e^{i\beta_{n,j-1}^o d_j}\end{bmatrix} \tag{18e}$$

$$\mathbf{T}_{j,j}^o=\begin{bmatrix}e^{-i\beta_{n,j}^o d_j} & e^{i\beta_{n,j}^o d_j}\\\frac{i\beta_{n,j}^o}{\varepsilon_j}e^{-i\beta_{n,j}^o d_j} & -\frac{i\beta_{n,j}^o}{\varepsilon_j}e^{i\beta_{n,j}^o d_j}\end{bmatrix}. \tag{18f}$$

The relation between $b_{n,1}^o$ and the vector $\mathbf{x}_{n,5}^o$ can be formulated as

$$\mathbf{x}_{n,5}^o = \begin{bmatrix} b_{n,5}^o \\ c_{n,5}^o \end{bmatrix} = \mathbf{T}^o b_{n,1}^o \tag{19}$$

The transfer matrix $\mathbf{T}^o$ is obtained as

$$\mathbf{T}^o = \left(\mathbf{T}_{5,5}^o\right)^{-1} \mathbf{T}_{4,5}^o \left(\mathbf{T}_{4,4}^o\right)^{-1} \mathbf{T}_{3,4}^o \left(\mathbf{T}_{3,3}^o\right)^{-1} \mathbf{T}_{2,3}^o \left(\mathbf{T}_{2,2}^o\right)^{-1} \mathbf{T}_1^o \tag{20}$$

and the nth column of $\mathbf{T}^o$ can be expressed as $[t_{1n}^o \quad t_{2n}^o]^T$. Substituting (19) into the continuity relations (4i) and (4j), we may write

$$\frac{a}{2}(t_{1r}^o + t_{2r}^o) b_{r,1}^o = \sum_{m=0}^{\infty} i g_m^o \mathbf{I}_{rm}^o \tag{21a}$$

$$\frac{b}{2} f_r^o = \sum_{n=0}^{\infty} i \beta_{n,5}^o (t_{1n}^o - t_{2n}^o) b_{n,1}^o \mathbf{I}_{nr}^o \tag{21b}$$

where

$$\mathbf{I}_{nm}^o = \frac{K_m^o}{(\gamma_n^o)^2 - (K_m^o)^2} \cos K_m^o a \sin \gamma_n^o a. \tag{21c}$$

By substituting $\alpha = \alpha_n^o$ in (15) and using (12a), we get infinitely many linear systems of equations with an infinite number of unknowns that give the constants f_n^o and g_n^o as follows:

$$\begin{aligned} \frac{b}{2i} \frac{(f_n^o + \alpha_n^o g_n^o)}{N_+^o(\alpha_n^o)} \frac{\sin K_n^o b}{\sqrt{k + \alpha_n^o}} = \quad & -2ie^{-ikb \sin \phi_0} \frac{\sqrt{k(1 - \cos \phi_0)}\, N_-^o(k \cos \phi_0)}{(\alpha_n^o - k \cos \phi_0)} \\ & + \sum_{m=0}^{\infty} \frac{(f_m^o - \alpha_m^o g_m^o)}{2\alpha_m^o} \frac{N_+^o(\alpha_m^o) \sqrt{k + \alpha_m^o}\, \sin K_m^o b}{(\alpha_n^o + \alpha_m^o)}, \end{aligned} \tag{22}$$

$n = 0,1,2, \cdots$.

B. EVEN EXCITATION

The solution for even excitation is obtained similar to the one for odd excitation. All the boundary and continuity conditions remain valid for the even excitation case, except (4b) and (4d), which are to be changed as

$$\frac{\partial}{\partial y} u_{2,j}^e(x, 0) = 0, \qquad x < 0 \tag{23a}$$

$$\frac{\partial}{\partial y} u_3^e(x, 0) = 0, \qquad x > 0. \tag{23b}$$

In this situation, MWHE-2 is obtained

$$\frac{F_+^e(\alpha, b)}{K^2 N^e(\alpha)} - F_-^e(\alpha, b) = -\frac{2ie^{-ikb \sin \phi_0}}{(\alpha - k \cos \phi_0)} + \sum_{m=0}^{\infty} (f_m^e + \alpha g_m^e) \frac{\cos K_m^e b}{K^2 - (K_m^e)^2} \tag{24}$$

with

$$N^e(\alpha) = K \sin Kb \; e^{iK(\alpha)b} \tag{25a}$$

$$p_m = \begin{cases} b/2, & m \neq 0 \\ b, & m = 0 \end{cases} \tag{25b}$$

$$K_m^e = K(\alpha_m^e) = \frac{m\pi}{b}, \qquad m = 0,1,2, \ldots \tag{25c}$$

$$\begin{bmatrix} f_m^e \\ g_m^e \end{bmatrix} = \frac{1}{p_m} \int_0^b \begin{bmatrix} f^e(t) \\ g^e(t) \end{bmatrix} \cos K_m^e t \, dt \tag{25d}$$

$N^e(\alpha)$ is the kernel function of (24) and factorized as [27]

$$N^e(\alpha) = N_+^e(\alpha) N_-^e(\alpha) \tag{26a}$$

$$N_+^e(\alpha) = N_-^e(-\alpha) \tag{26b}$$

where

$$\begin{aligned} N_+^e(\alpha) = & \sqrt{\frac{\sin kb}{k}} \exp\left\{\frac{ib\alpha}{\pi}\left(1 - C + \ln\left(\frac{2\pi}{kb}\right) + i\frac{\pi}{2}\right)\right\} \\ & \times \exp\left\{\frac{ibK}{\pi} \ln\left(\frac{\alpha + K}{k}\right)\right\} \prod_{m=1}^{\infty} \left(1 + \frac{\alpha}{\alpha_m}\right) \exp\left\{\frac{i\alpha b}{m\pi}\right\}. \end{aligned} \tag{26c}$$

WHE is solved by following classical steps and one gets

$$\frac{\dot{F_+^e}(\alpha, b)}{K^2 N_+^e(\alpha)} = \tilde{F}_+^e(\alpha, b) \tag{27a}$$

with

$$\begin{aligned} \tilde{F}_+^e(\alpha, b) = & -2ie^{-ikb \sin \phi_0} \frac{k(1 - \cos \phi_0) N_-^e(k \cos \phi_0)}{(\alpha - k \cos \phi_0)} \\ & + \sum_{m=0}^{\infty} \frac{(f_m^e - \alpha_m^e g_m^e)}{2\alpha_m^e} \frac{(k + \alpha_m^e) N_+^e(\alpha_m^e) \cos K_m^e b}{(\alpha + \alpha_m^e)} \end{aligned} \tag{27b}$$

$$\dot{F_+^e}(\alpha_n^e, b) = p_n \cos K_n^e b \, (f_n^e + \alpha_n^e g_n^e) \tag{27c}$$

Similar to the odd excitation case, in the waveguide region $0 < y < a, x < 0$, $u_{2,j}^o(x, y)$ should be expressed separately for each layer and can be given as

$$u_{2,j}^e(x, y) = \sum_{n=0}^{\infty} \left[b_{n,j}^e e^{i\beta_{n,j}^e x} + c_{n,j}^e e^{-i\beta_{n,j}^e x} \right] \cos \gamma_n^e y, \qquad j = 1,2, \ldots, 5 \tag{28a}$$

$$\gamma_n^e = \frac{n\pi}{a}, \qquad n = 0,1,2, \ldots \tag{28b}$$

$$\beta_{n,j}^{e} = \sqrt{k_j^2 - (\gamma_n^e)^2}\,. \tag{28c}$$

where $k_j = k\sqrt{\varepsilon_j \mu_j}$, j denotes the jth layer. When $u_{2,1}^{e}(x,y)$ is replaced at the boundary condition at $x = -d_1$ and one gets

$$u_{2,1}^{e}(x,y) = \sum_{n=0}^{\infty} b_{n,1}^{e} \sin\beta_{n,1}^{e}(x+d_1)\cos\gamma_n^e y \tag{29}$$

Once we substitute the field expressions $u_{2,j}^{e}(x,y)$ into the continuity relations (4g) and (4h) for each layer, we get

$$\mathbf{T}_1^e b_{n,1}^{e} = \mathbf{T}_{2,2}^{e}\mathbf{x}_{n,2}^{e} \tag{30a}$$

$$\mathbf{T}_{j-1,j}^{e}\mathbf{x}_{n,j-1}^{e} = \mathbf{T}_{j,j}^{e}\mathbf{x}_{n,j}^{e}, \qquad j = 3{,}4{,}5 \tag{30b}$$

where

$$\mathbf{x}_{n,j}^{e} = \begin{bmatrix} b_{n,j}^{e} \\ c_{n,j}^{e} \end{bmatrix} \tag{30c}$$

$$\mathbf{T}_1^e = \begin{bmatrix} \cos\beta_{n,1}^{e}(d_1 - d_2) \\ -\dfrac{\beta_{n,1}^{e}}{\varepsilon_1}\sin\beta_{n,1}^{e}(d_1 - d_2) \end{bmatrix} \tag{30d}$$

$$\mathbf{T}_{j-1,j}^{e} = \begin{bmatrix} e^{-i\beta_{n,j-1}^{e}d_j} & e^{i\beta_{n,j-1}^{e}d_j} \\ \dfrac{i\beta_{n,j-1}^{e}}{\varepsilon_{j-1}}e^{-i\beta_{n,j-1}^{e}d_j} & -\dfrac{i\beta_{n,j-1}^{e}}{\varepsilon_{j-1}}e^{i\beta_{n,j-1}^{e}d_j} \end{bmatrix} \tag{30e}$$

$$\mathbf{T}_{j,j}^{e} = \begin{bmatrix} e^{-i\beta_{n,j}^{e}d_j} & e^{i\beta_{n,j}^{e}d_j} \\ \dfrac{i\beta_{n,j}^{e}}{\varepsilon_{j}}e^{-i\beta_{n,j}^{e}d_j} & -\dfrac{i\beta_{n,j}^{e}}{\varepsilon_{j}}e^{i\beta_{n,j}^{e}d_j} \end{bmatrix} \tag{30f}$$

The relation between $b_{n,1}^{e}$ and the vector $\mathbf{x}_{n,5}^{e}$ can be formulated as follows:

$$\mathbf{x}_{n,5}^{e} = \begin{bmatrix} b_{n,5}^{e} \\ c_{n,5}^{e} \end{bmatrix} = \mathbf{T}^{e} b_{n,1}^{e}. \tag{31}$$

The transfer matrix $\mathbf{T}^e$ for even excitation is obtained as

$$\mathbf{T}^e = \left(\mathbf{T}_{5,5}^{e}\right)^{-1}\mathbf{T}_{4,5}^{e}\left(\mathbf{T}_{4,4}^{e}\right)^{-1}\mathbf{T}_{3,4}^{e}\left(\mathbf{T}_{3,3}^{e}\right)^{-1}\mathbf{T}_{2,3}^{e}\left(\mathbf{T}_{2,2}^{e}\right)^{-1}\mathbf{T}_1^e \tag{32}$$

and n'th column of $\mathbf{T}^e$ can be expressed as $[t_{1n}^{e} \quad t_{2n}^{e}]^T$. Substituting (31) into the continuity relations (4i) and (4j), we may write

$$i\beta_{n,5}^{e}\frac{a}{2}\left(b_{n,5}^{e} - c_{n,5}^{e}\right) = \sum_{m=0}^{\infty} f_m^e\, I_{nm}^{e} \tag{33a}$$

$$ig_m^e\frac{b}{2} = \sum_{n=0}^{\infty}\left(b_{n,5}^{e} + c_{n,5}^{e}\right) I_{mn}^{e} \tag{33b}$$

where

$$I_{nm}^{e} = \frac{K_m^e}{(K_m^e)^2 - (\gamma_n^e)^2} \sin K_m^e a \cos \gamma_n^e a. \tag{33c}$$

By replacing $\alpha = \alpha_n^e$ in (27a) and using (27c), we get the following equations

$$p_n \frac{(f_n^e + \alpha_n^e g_n^e)}{N_+^e(\alpha_n^e)} \frac{\cos K_n^e b}{k + \alpha_n^e} = -2ie^{-ikb\sin\phi_0} \frac{k(1-\cos\phi_0) N_+^e(-k\cos\phi_0)}{(\alpha_n^e - k\cos\phi_0)} + \sum_{m=0}^{\infty} \frac{(f_m^e - \alpha_m^e g_m^e)}{2\alpha_m^e} \frac{(k+\alpha_m^e) N_+^e(\alpha_m^e) \cos K_m^e b}{(\alpha_n^e + \alpha_m^e)} \tag{34}$$

$n = 0,1,2,\cdots$.

C. ANALYSIS OF THE SCATTERED FIELD

The scattered field for odd and even excitations can be obtained by taking the inverse Fourier transform of $F^o(\alpha, y)$ and $F^e(\alpha, y)$, respectively

$$u_1^o(x,y) = \frac{1}{2\pi i} \int_{\mathcal{L}} \frac{\dot{F}_+^o(\alpha, b)}{K(\alpha)} e^{i[K(\alpha)(y-b) - \alpha x]} d\alpha \tag{35a}$$

$$u_1^e(x,y) = \frac{1}{2\pi i} \int_{\mathcal{L}} \frac{\dot{F}_+^e(\alpha, b)}{K(\alpha)} e^{i[K(\alpha)(y-b) - \alpha x]} d\alpha, \tag{35b}$$

where $\mathcal{L}$ is a straight line parallel to the real axis lying in the strip $\Im m(k\cos\phi_0) < \Im m(\alpha) < \Im m(k)$. The evaluation of the integrals in (35a) and (35b) by using the method of saddle-point technique yields the asymptotic expression of $u_1\ (r, \phi)$ for the far field as follows

$$u_1\ (r,\phi) = \frac{u_1^e(r,\phi) + u_1^o(r,\phi)}{2} \tag{36a}$$

with

$$u_1^o(r,\phi) = \frac{e^{-i\pi/4}}{\sqrt{2\pi}} \tilde{F}_+^o(-k\cos\phi\ , b)\ N_-^o(k\cos\phi) \sqrt{k(1-\cos\phi)} \frac{e^{ikr}}{\sqrt{kr}} \tag{36b}$$

$$u_1^e(r,\phi) = \frac{e^{-i3\pi/4}}{\sqrt{2\pi}} \tilde{F}_+^e(-k\cos\phi\ , b)\ N_-^e(k\cos\phi)\ k(1-\cos\phi)\ \frac{e^{ikr}}{\sqrt{kr}} \tag{36c}$$

where (r, ϕ) cylindrical polar coordinates are defined by

$$x = r\cos\phi\ , \quad y - b = r\sin\phi\ . \tag{36d}$$

III. NUMERICAL RESULTS

This section focuses on the numerical results for the far-field backscattering properties of the cavities for the RCS examples. The definition of the RCS is given per unit length in the literature as follows

$$\sigma = \lim_{r\to\infty}\left(2\pi r\frac{|u_1|^2}{|u^i|^2}\right), \tag{37}$$

where u_1 is the diffracted field and u^i is the incident field defined by (36a) and (2a), respectively. The method that is applied by incorporating the modal expressions of the field in the waveguide region for each layer separately allows one the flexibility to choose the number of the dielectric layers for the reduction of the RCS, easily. In addition, the results that are presented here show the importance of the wall thickness of the cavity in the calculation of monostatic RCS which is calculated only in the opposite direction of the incident field, and have been given for different wall thicknesses by comparing the results presented in [25] for the same dielectric parameters.

Table 1. *Characteristics of the materials that fill the cavity*

Layer,j	$\boldsymbol{\varepsilon_j}$	$\boldsymbol{\mu_j}$
1	$3.14 + i10$	$1 + i0$
2	$1.6 + i0.9$	$1 + i0$
3	$1.4 + i0.35$	$1 + i0$
4	$2.4 + i1.25$	$1.6 + i1.9$
5	$1 + i0$	$1 + i0$

The layer thicknesses are taken as equal to each other, namely $t = d_n - d_{n+1},\ n = 1,2,3,4$ to compare our results with [25]. The material properties are listed in Table 1 and the numerical results are derived for four distinct cases: vacuum, one-layer, three-layer, and four-layer material loadings.

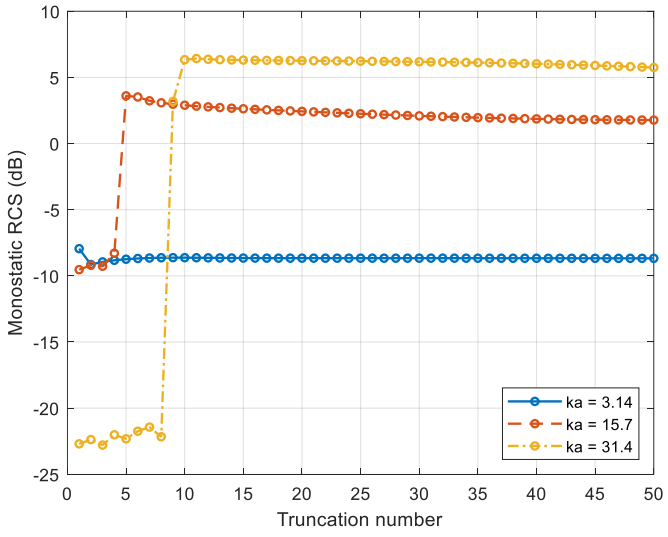

Figure 4. *The monostatic RCS versus the truncation number for* $\phi = 60^{\circ}$ *(*$kb = ka + 0.314$, $d_1/2a = 1$, $kt = 0.628$, *three-layer material)*

Figure 4 shows the stability of the results for the diffracted field with the truncation number, *N*, of the infinite number of linear systems of equations. The scattered field becomes insensitive to the truncation number when *N>10* even for different waveguide dimensions.

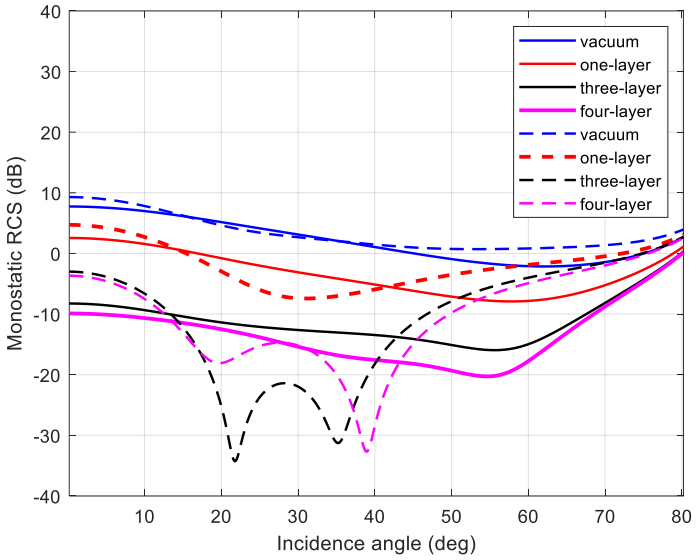

Figure 5. *Comparison of the results for different wall thicknesses, —— b/a=1, - - - b/a=1.2*

The normalized monostatic RCS as a function of the incident angle ϕ_0 is given in Figures 5 – 10. Figure 5 represents the effect of the wall thickness for the RCS calculation by comparing the results given in [25] where the plates are considered very thin. Our results show that between around 15 to 45-degree incidence angle, the RCS gets better. In addition, Figure 6 shows the variation of RCS for different wall thicknesses that RCS increases or decreases up to 20 dB for different angles of incidence. Figures 7, 8, 9, and 10 are regenerated for the same dielectric parameters as in [25] to show the variation of RCS when the wall thickness is taken into account.

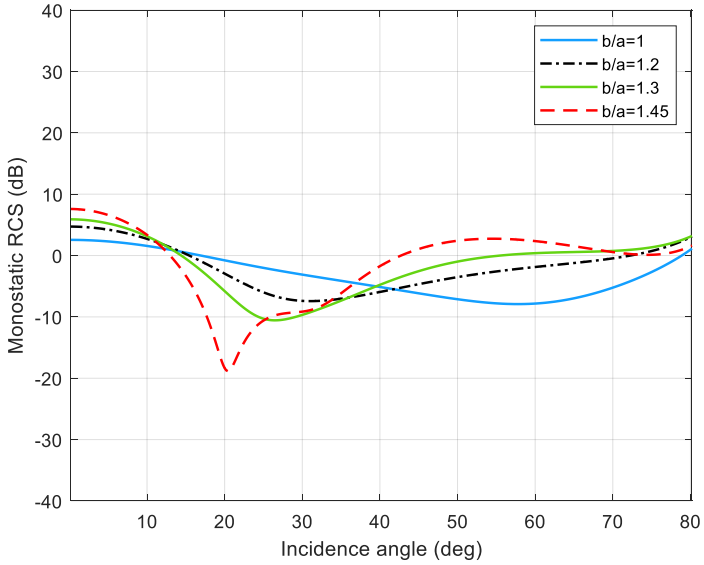

Figure 6. *Monostatic RCS for one layer loading case. Properties of the structure are* $d_1/2a = 1$, $ka = 3.14$, $kt = 0.628$

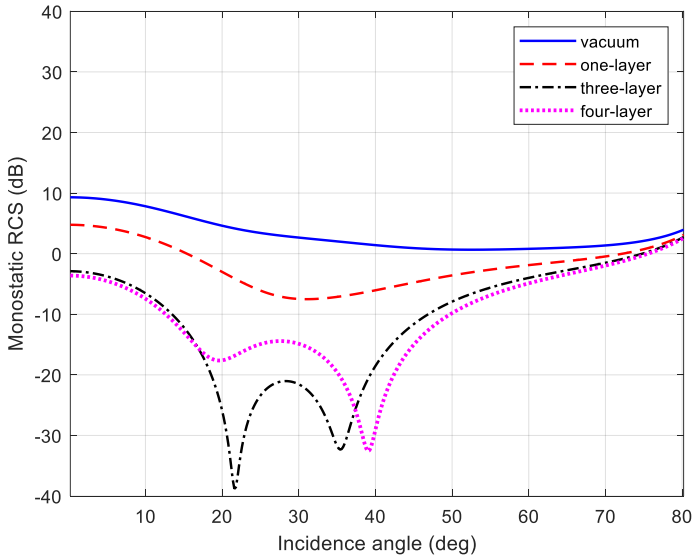

(a)

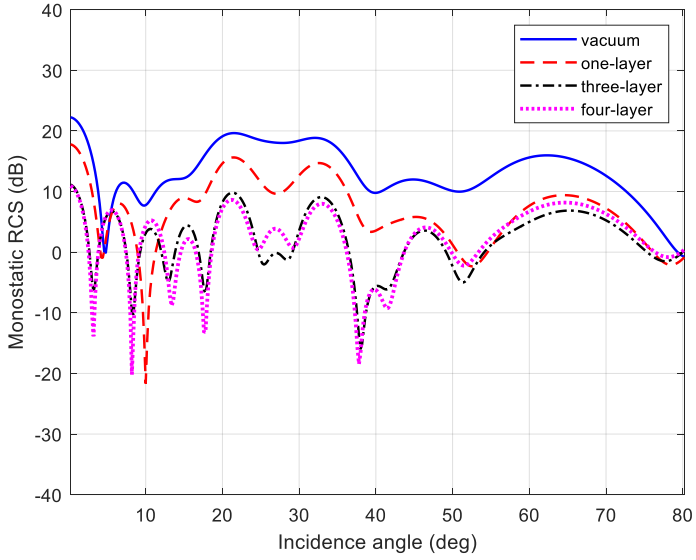

(b)

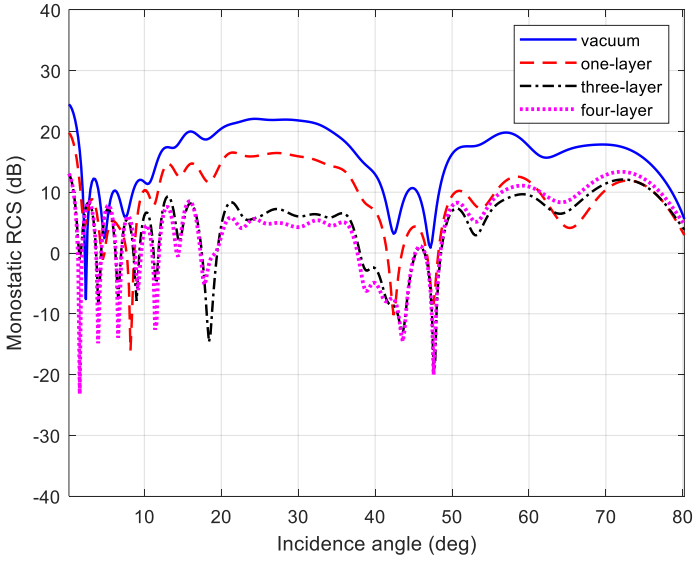

(c)

Figure 7. *Monostatic RCS for* ***(a)*** $\mathrm{ka} = 3.14$ ***(b)*** $\mathrm{ka} = 15.7$ ***(c)*** $\mathrm{ka} = 31.4$ ***(*** $b/\mathrm{a} = 1.2$, $\mathrm{d}_1/2\mathrm{a} = 1$, $\mathrm{kt} = 0.628$ *for all cases****)***

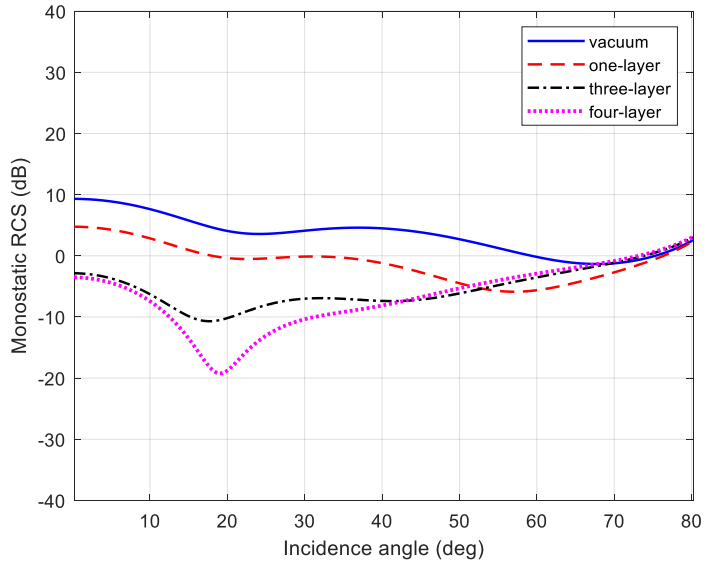

(a)

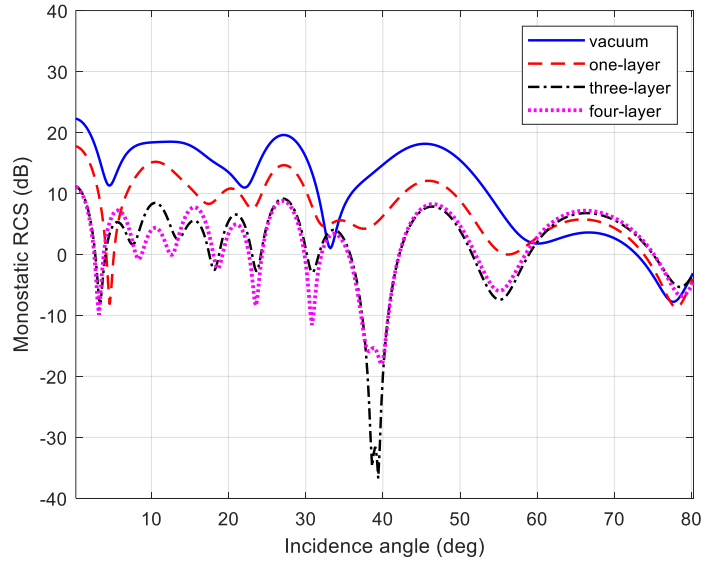

(b)

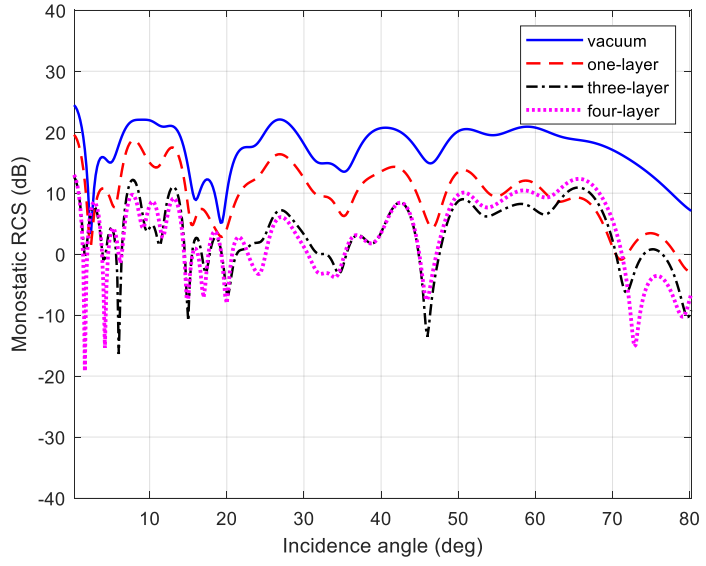

(c)

Figure 8. *Monostatic RCS for* ***(a)*** $\mathrm{ka} = 3.14$ ***(b)*** $\mathrm{ka} = 15.7$ ***(c)*** $\mathrm{ka} = 31.4$ *(*$b/\mathrm{a} = 1.2$, $\mathrm{d}_1/2\mathrm{a} = 3$, $\mathrm{kt} = 0.628$, *for all cases)*

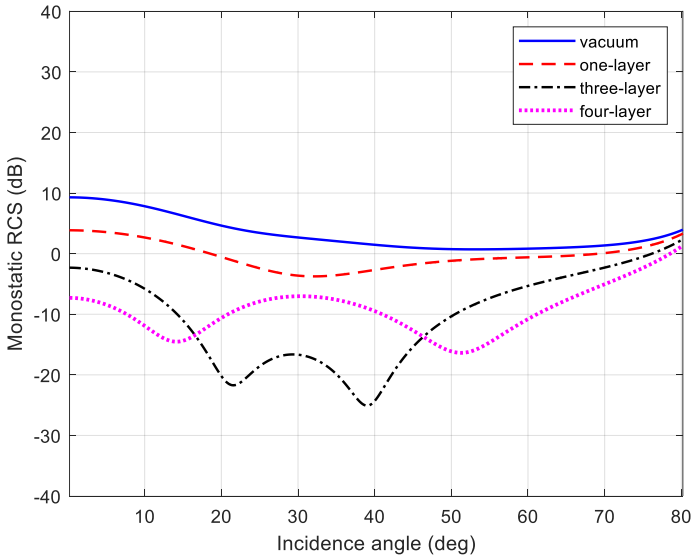

(a)

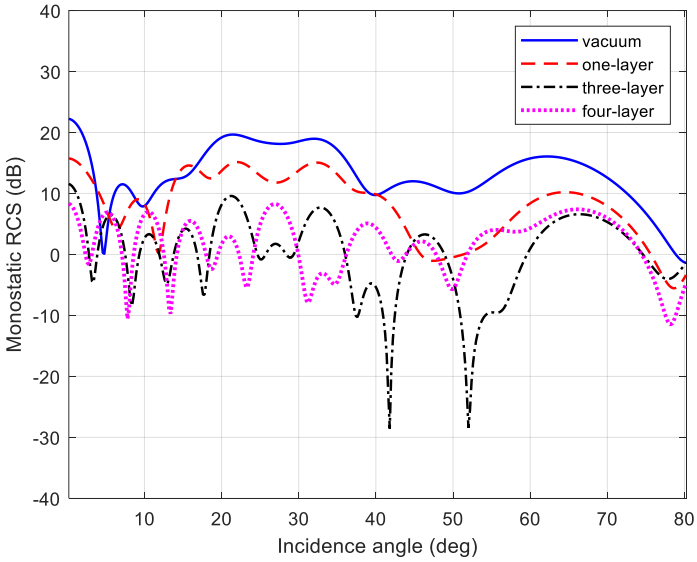

(b)

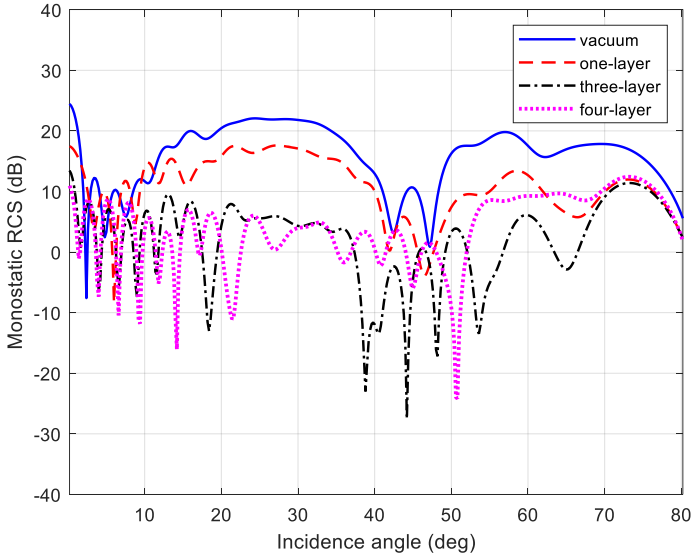

(c)

Figure 9. *Monostatic RCS for* ***(a)*** ka = 3.14 ***(b)*** ka = 15.7 ***(c)*** ka = 31.4 *(*$b/\mathrm{a} = 1.2$, $\mathrm{d}_1/2\mathrm{a} = 1$, kt = 1.255 *for all cases)*

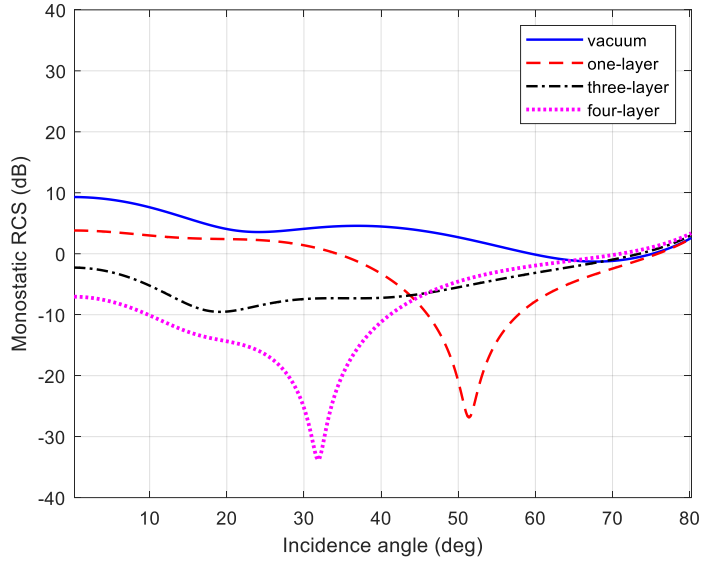

(a)

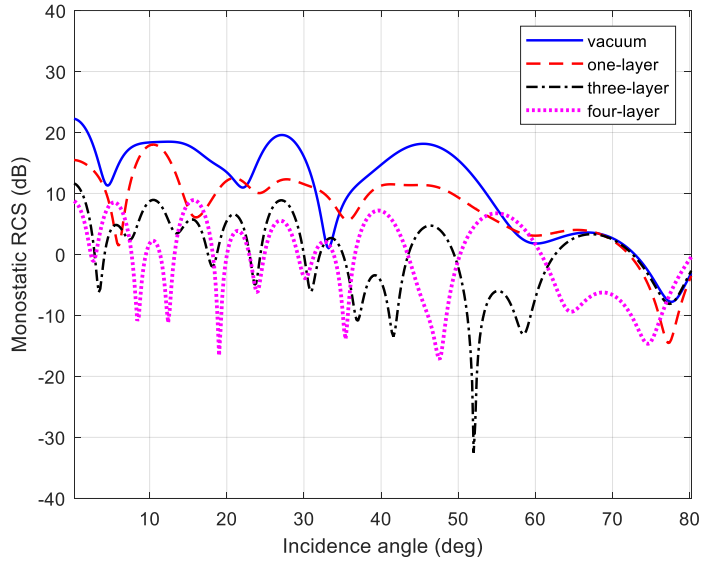

(b)

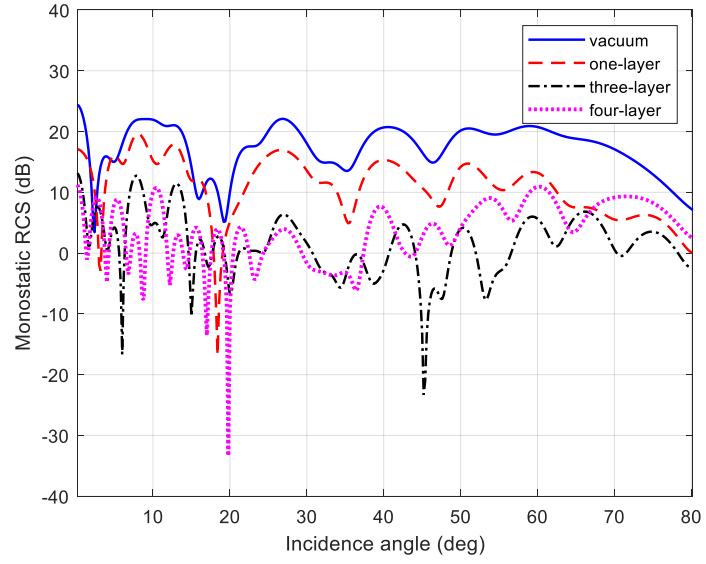

(c)

Figure 10. *Monostatic RCS for* ***(a)*** $\mathrm{ka} = 3.14$ ***(b)*** $\mathrm{ka} = 15.7$ ***(c)*** $\mathrm{ka} = 31.4$ *(*$b/\mathrm{a} = 1.2$, $\mathrm{d}_1/2\mathrm{a} = 3$, $\mathrm{kt} = 1.255$ *for all cases)*

IV. CONCLUSION

In this paper, we analyzed the effect of the wall thickness on the radar cross-section of the material-loaded planar waveguide which is terminated with a PEC plate to form a cavity. The scattering problem is formulated as the solution of two uncoupled MWHE-2's. These equations are solved by incorporating the modal expansions of the field in the waveguide region to form a linear system of equations. As a result, the scattered field is obtained after applying the inverse Fourier transform to two spectral functions $F^o(\alpha, y)$ and $F^e(\alpha, y)$. The analysis allows one to take into account the wall thickness of the plates and the flexibility to change the number and the thickness of layers with different dielectric parameters. The numerical results that are given to reflect the effect of wall thickness show that it is an important parameter for RCS reduction studies. Depending on the cavity wall thickness, RCS might be up to 20 dB higher or lower. In addition, it has been shown that when the number of the dielectric layers increased, RCS gets better also for the case of thick cavity wall.

V. REFERENCES

[1] C. Lee and S.-W. Lee, "RCS of a coated circular waveguide terminated by a perfect conductor," *IEEE Transactions on Antennas and Propagation*, vol. 35, no. 4, pp. 391-398, 1987.

[2] A. Altintas, P. H. Pathak and M.-C. Liang, "A selective modal scheme for the analysis of EM coupling into or radiation from large open-ended waveguides," *IEEE Transactions on Antennas and Propagatio*n, vol. 36, no. 1, pp. 84-96, 1988.

[3] N. N. Youssef, "Radar cross-section of complex targets," *Proceedings of the IEEE*, vol. 77, no. 5, pp. 722-734, 1989.

[4] W. R. Stone, *Radar Cross-Sections of Complex Objects*, New York: IEEE Press, 1990.

[5] A. Demir, A. Büyükaksoy and B. Polat, "Diffraction of plane sound waves by a rigid circular cylindrical cavity with an acoustically absorbing internal surface," *ZAMM Z. Angew. Math. Mech.*, vol. 82, no. 9, pp. 619-629, 2002.

[6] Y.-D. Kim, H. Lim, J.-H. Han, W.-Y. Song, and N.-H. Myung, "RCS reduction of open-ended circular waveguide cavity with corrugations using mode matching and scattering matrix analysis," *Progress in Electromagnetics Research*, vol. 146, pp. 57-69, 2014.

[7] G. Bao and J. Lai, "Optimal shape design of a cavity for radar cross-section reduction," *SIAM Journal on Control and Optimization*, vol. 52, no.4, pp. 2122-2140, 2014.

[8] B. Tiryakioglu and A. Demir, "Radiation analysis of sound waves from semi-infinite coated pipe," *International Journal of Aeroacoustics*, vol. 18, no. 1, pp. 92-111, 2019.

[9] P. H. Pathak and R. J. Burkholder, "Modal, ray, and beam techniques for analyzing the EM scattering by open-ended waveguide cavities," *IEEE Transactions on Antennas and Propagation*, vol. 37, no. 5, pp. 635-647, 1989.

[10] H. Ling, S.-W. Lee and R.-C. Chou, "High-frequency RCS of open cavities with rectangular and circular cross-sections," *IEEE Transactions on Antennas and Propagation*, vol. 37, no. 5, pp. 648-654, 1989.

[11] G. Bao and J. Lai, "Radar cross-section seduction of a cavity in the ground plane," *Communications in Computational Physics*, vol. 15, no.4, pp. 895-910, 2014.

[12] E. Vinogradova, "Electromagnetic plane wave scattering by arbitrary two-dimensional cavities: Rigorous approach," *Wave Motion*, vol. 70, pp. 47-64, 2017.

[13] Y. Zhou, et al. "Broadband RCS reduction for electrically-large open-ended cavity using random coding metasurfaces," *Journal of Physics D: Applied Physics*, vol. 52, 2019.

[14] S. Koshikawa, D. Colak, A. Altintas, K. Kobayashi, and A.I. Nosich, "A comparative study of RCS predictions of canonical rectangular and circular cavities with double-layer material loading," *IEICE Transactions on Electronics*, vol. E80-C, no.11, pp. 1457–1466, 1997.

[15] K. Kobayashi and A. Sawai, "Plane wave diffraction by an open-ended parallel plate waveguide cavity," *Journal of Electromagnetic Waves and Applications*, vol. 6, no.1-4, pp. 475–512, 1992.

[16] K. Kobayashi, S. Koshikawa, and A. Sawai, "Diffraction by a parallel-plate waveguide cavity with dielectric/ferrite loading: Part I - The case of E polarization," *Progress in Electromagnetics Research*, vol. 8, pp. 377-426, 1994.

[17] S. Koshikawa and K. Kobayashi, "Diffraction by a parallel-plate waveguide cavity with dielectric/ferrite loading: Part II - The case of H polarization," *Progress in Electromagnetics Research*, vol. 8, pp. 427–458, 1994.

[18] J.P. Zheng and K. Kobayashi, "Plane wave diffraction by a finite parallel-plate waveguide with four-layer material loading: Part I - The case of E polarization," *Progress in Electromagnetics Research B*, vol. 6, pp. 1–36, 2008.

[19] E.H. Shang and K. Kobayashi, "Plane wave diffraction by a finite parallel-plate waveguide with four-layer material loading: Part II - The case of H polarization," *Progress in Electromagnetics Research B*, vol. 6, pp. 267–294, 2008.

[20] S. Koshikawa and K. Kobayashi, "Diffraction by a terminated semi-infinite parallel-plate waveguide with three-layer material loading," *IEEE Transactions on Antennas and Propagation*, vol. 45, no. 6, pp. 949-959, 1997

[21] S. Koshikawa and K. Kobayashi, "Diffraction by a terminated, semi-infinite parallel-plate waveguide with three-layer material loading: The case of H polarization," *Telecommunications and Radio Engineering*, vol. 54, no. 3, pp. 13–23, 2000.

[22] A. Büyükaksoy and B. Polat, "Plane wave diffraction by a thick-walled parallel-plate impedance waveguide," *IEEE Transactions on Antennas and Propagation*, vol. 46, no. 11, pp. 1692-1699, 1998.

[23] M. Dumanli, "Diffraction by a terminated semi-infinite parallel plate waveguide with two-layer material loading and impedance boundaries," *Progress in Electromagnetics Research*, vol. 45, pp. 77-102, 2004.

[24] E.H. Shang and K. Kobayashi, "Diffraction by a terminated, semi-infinite parallel-plate waveguide with four-layer material loading: The case of H polarization," *Progress in Electromagnetics Research B*, vol. 12, pp. 139–162, 2009.

[25] K. He and K. Kobayashi, "Diffraction by a semi-infinite parallel-plate waveguide with five-layer material loading: The case of H-polarization," *Applied Sciences*, vol. 13, no. 6, pp. 3715, 2023.

[26] R. Mittra and S.-W. Lee, *Analytical Techniques in the Theory of Guided Waves*, New York: Macmillan, 1971.